

See discussions, stats, and author profiles for this publication at: <https://www.researchgate.net/publication/335874249>

Machine Learning (ML)–Assisted Design and Fabrication for Solar Cells

Article in *Energy & Environmental Materials* · September 2019

DOI: 10.1002/eeem2.12049

CITATIONS

20

READS

371

7 authors, including:



Minlin Jiang

University of Pittsburgh

42 PUBLICATIONS 522 CITATIONS

[SEE PROFILE](#)



Min Xu

Carnegie Mellon University

93 PUBLICATIONS 1,404 CITATIONS

[SEE PROFILE](#)

Some of the authors of this publication are also working on these related projects:



In situ Cryo-electron tomography [View project](#)



Perovskite solar cell [View project](#)

Machine Learning (ML)-Assisted Design and Fabrication for Solar Cells

Fan Li, Xiaoqi Peng, Zuo Wang, Yi Zhou, Yuxia Wu, Minlin Jiang*, , and Min Xu*

Photovoltaic (PV) technologies have attracted great interest due to their capability of generating electricity directly from sunlight. Machine learning (ML) is a technique for computer to learn how to perform a specific task using known data. It can be used in many areas and has become a hot research topic recently due to the rapid accumulation of data and advancement of computer hardware. The application of ML techniques in the design and fabrication of solar cells started slowly but has recently gained tremendous momentum. An exhaustive compilation of the literatures indicates that all the major aspects in the research and development of solar cells can be effectively assisted by ML techniques. If combined with other tools and fed with additional theoretical and experimental data, more accurate and robust results can be achieved from ML techniques. The aspects can be grouped into four categories: prediction of material properties, optimization of device structures, optimization of fabrication processes, and reconstruction of measurement data. A statistical analysis of the literatures shows that artificial neural network (ANN) and genetic algorithm (GA) are the two most applied ML techniques and the topics in the optimization of device structures and optimization of fabrication processes are more popular. This article can be used as a reference by all PV researchers who are interested in ML techniques.

1. Introduction

Photovoltaic (PV) technologies have attracted great interest due to their capability of generating electricity directly from sunlight.^[1] As a core element in PV technologies and being developed for decades, solar cell has gained significant progress in terms of efficiency.^[2] Generation after generation of solar cells have been designed, developed, and deployed.^[3–5] Development of a typical solar cell includes three major aspects: finding the appropriate PV materials, optimizing the device

structures, and developing the fabrication processes. Most of the experimental development procedures employ a trial-and-error approach, which is expensive and time-consuming due to vast numbers of parameters to be considered. Theoretical calculations based on first principle,^[6,7] density function theory (DFT),^[8,9] and Monte Carlo^[10,11] have been successfully applied to the above-mentioned aspects. However, complicated models and a significant amount of data and computing time are required.^[12]

Machine learning (ML) is a technique for computers to learn how to conduct a specific task from known data.^[13,14] It can be used in many areas and has become a hot research topic recently due to the rapid accumulation of data and advancement of computer hardware.^[15–18] The application of ML techniques in the design and fabrication of solar cells started slowly but has recently gained tremendous momentum.^[19,20] This article comprehensively reviews the application of ML techniques applied in solar cells in the following four aspects: prediction of material properties, optimization of device structures, optimization of fabrication processes, and reconstruction of measurement

data. The research topics are categorized in this article so that researchers can track the trend of ML techniques applied in the field of solar cells.


2. Typical ML Techniques In Solar Cells

This section briefly introduces most of the ML techniques used to optimize the design and fabrication of solar cell.

2.1. Artificial Neural Network (ANN)

ANN is a directed acyclic graph computation model used for learning complex rules from big data.^[21,22] Tasks such as pattern recognition,^[23] data classification,^[24] and performance prediction^[25] can be generally performed through a learning from examples without specific rules being hand-programmed. An ANN consists of a couple of layers where nodes called artificial neurons are connected and aggregated.^[26] The artificial neurons can receive, process, and transmit signals according to different algorithms. The typical ANN model consists of three layers, which are called input layer, hidden layer, and output layer, respectively (**Figure 1**). The neurons in the input layer receive the raw information that is fed

F. Li, X. Peng, Y. Wu, Prof. M. Jiang
Institute of Advanced Study, Nanchang University, Nanchang Jiangxi 330031, China
E-mail: minlinjiang@ncu.edu.cn
Z. Wang, Y. Zhou
School of Information Engineering, Nanchang University, Nanchang Jiangxi 330031, China
Prof. M. Xu
Department of Computational Biology, Carnegie Mellon University, Pittsburgh PA 15213, USA
E-mail: mxu1@andrew.cmu.edu

 The ORCID identification number(s) for the author(s) of this article can be found under <https://doi.org/10.1002/eem2.12049>.

DOI: 10.1002/eem2.12049

into the network, and the neurons in the hidden layer and in the output layer process the information. The outputs of the neurons in the hidden layer are determined by the activities of the neurons in the input layer and the weights on the connections between the input neurons and the hidden neurons. The outputs of the neurons in the output layer depend on the activity of the neurons in the hidden layer and the weights between the hidden neurons and output neurons.

2.2. Genetic Algorithm (GA)

The GA is a method that imitates the natural selection and can solve both unconstrained and constrained optimization problems.^[27,28] An initial population of genes is selected in this algorithm. Selection rules are designed to select the individuals which are called as “parents” and will contribute to the population at the next generation which are usually called as “children” (Figure 2). Crossover rules and mutation rules are used to produce the children with the best fitness function values. A population of individual solutions can be repeatedly modified in the GA and will evolve toward an optimal solution. GA can be applied to solve optimization problems whose objective functions are discontinuous, stochastic, nondifferentiable, stochastic, or highly nonlinear. Complex optimization tasks in pattern recognition,^[29] image enhancement and segmentation,^[30,31] traffic signal coordination,^[32] software testing,^[33] intrusion detection,^[34] and unmanned aerial vehicles (UAV)^[35] can be performed by GA.

2.3. Particle Swarm Optimization (PSO)

PSO is a computational method inspired by a swarm of flying birds that are searching for food (Figure 3).^[36] Each bird in the group moves in a direction based on its experience and group movements until they finally converge in a specific location where they find the food. In PSO, a population of candidate solutions are called as particles, which act like the birds, and the best solution to a problem can be obtained by

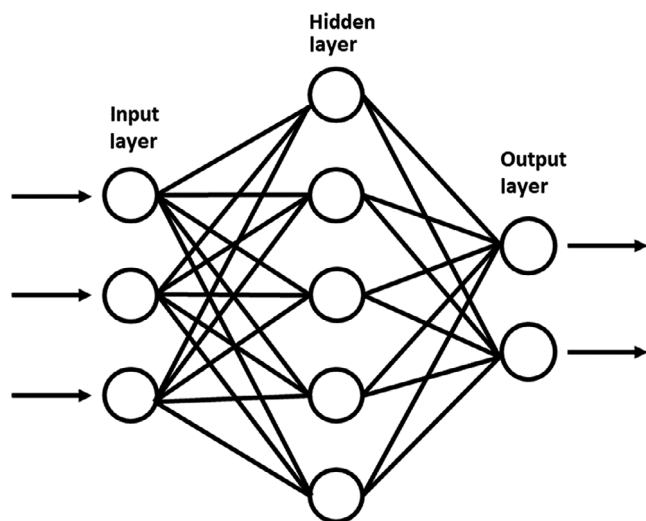


Figure 1. Structure of an artificial neural network.



Minlin Jiang received the B.S. degree in Physics from Jiangxi Normal University, Nanchang, China, in 2000, and the M.S. degree in Optical Engineering from Shanghai Jiaotong University, Shanghai, China, in 2009. He has also received another M.S. degree in Electrical Engineering from South Dakota State University, Brookings, SD, USA, in 2012.

He earned the Ph.D. degree in Electrical Engineering from University of Pittsburgh, Pittsburgh, PA, USA, in 2017. He is currently a Professor in Nanchang University, Nanchang, Jiangxi, China. His research interests include inorganic compound solar cells, gas sensors, and the application of artificial intelligence in PV technologies.

iteratively updating the positions of these particles in the search space according to simple mathematical formula.^[37] PSO algorithms have been used in the path planning for the UAV robots,^[38] watermarking in digital image,^[39] the management of groundwater resources,^[40] and the optimization of the radio-frequency identification (RFID) network with redundant reader elimination.^[41]

2.4. Simulated Annealing (SA)

SA algorithm mimics the annealing process of materials where the temperature of the materials is deliberately decreased to increase the crystal size of the materials and reduce their defects.^[42] It is often applied to search for a global optimum in a large search space. SA algorithm is better than other algorithms such as gradient descent if the search space is discrete, and finding the approximate global optimum is more important than finding an accurate local optimum. Generally, a solution close to the current one is randomly chosen in SA algorithm with a relatively high temperature (Figure 4). The current solution will either be replaced by the randomly chosen solution or stay depending on the two possibilities: the possibility of moving to a new and better solution and possibility of moving to a new and worse solution. The temperature is gradually decreased from the initial value to zero, which affects the two possibilities. SA can be applied to various fields such as very large-scale integration (VLSI),^[43] production scheduling,^[44] control engineering,^[45] machine learning,^[46] signal processing,^[47] and image reconstruction.^[48]

2.5. Random Forest (RF)

RF is a method to create a relatively strong classifier by combining many decision trees which are relatively weak classifiers and not related.^[49] These decision trees are constructed from random subsample of features. The final predicted classification of an object in the RF is obtained by averaging the predictions of the individual trees (Figure 5). RF can be applied to marketing,^[50] health care,^[51] and risk management.^[52,53]

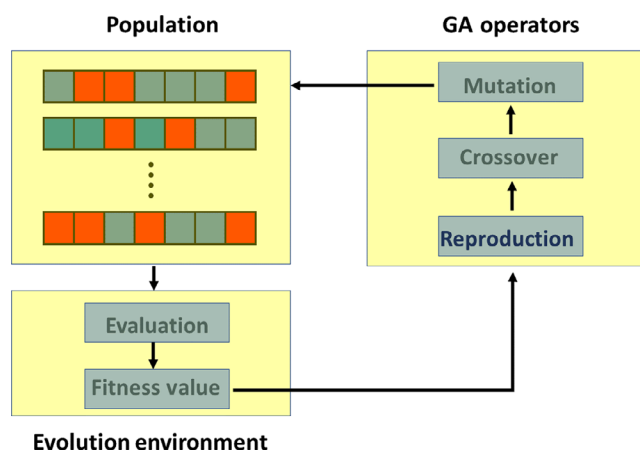


Figure 2. Structure of genetic algorithm.

2.6. Other ML Techniques

Except for the above-mentioned ML techniques, other ML techniques have also been occasionally applied to assist the design and fabrication of solar cell. These methods include support vector machine (SVM),^[54] kernel ridge regression (KRR),^[55] extremely randomized trees (ERT),^[56] k nearest neighbors (kNN),^[57] gradient boosting (GB),^[58] ant colony algorithm (ACA),^[59] evolutionary algorithm (EA),^[60] squared-exponential kernel (SEK),^[61] decision tree (DT),^[62] fuzzy logic (FL),^[63] adaptive boosting (AB),^[64] vortex component analysis (VCA),^[65] and non-negative matrix factorization (NNMF).^[66]

3. Applications of ML Techniques in Solar Cells

ML techniques are used in various aspects of solar cells, such as design, fabrication, and characterization. The applications of ML techniques in

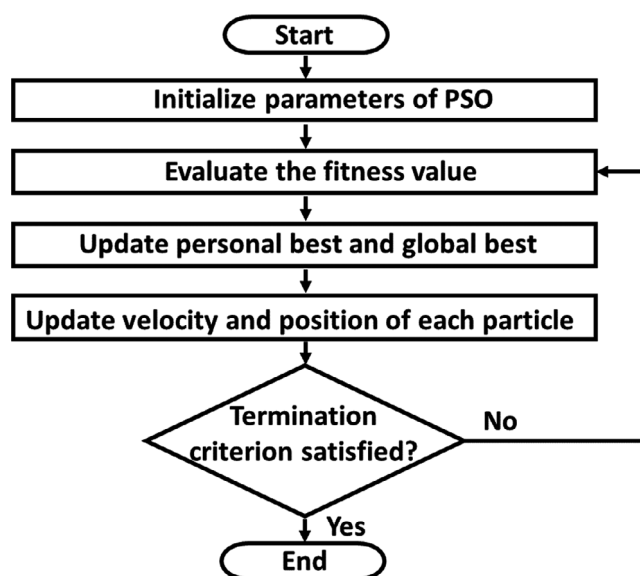


Figure 3. Structure of particle swarm optimization algorithm.

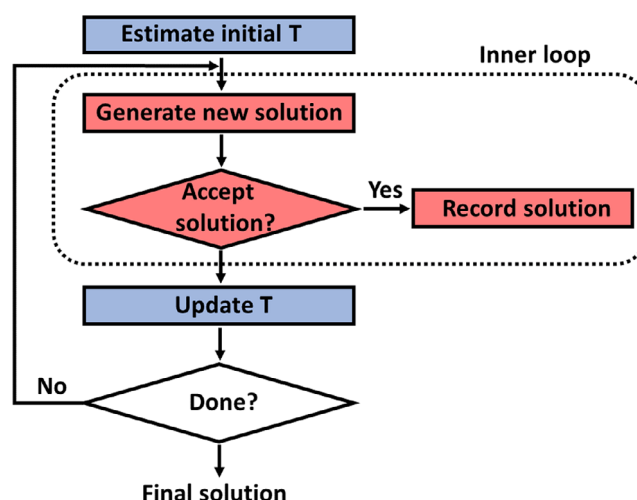


Figure 4. Structure of simulated annealing algorithm.

the research and development of solar cells can be classified into five major categories: prediction of material properties, optimization of device structures, optimization of fabrication processes, reconstruction of measurement data, and extraction of parameters of solar cell models. For the application of ML techniques in extracting parameters of solar cell models, we recommend reference^[67] where the readers can find a brief review on this topic. The other four applications will be thoroughly introduced in the following sections.

3.1. Prediction of Material Properties

The identification of suitable materials for solar cells is challenging due to a large space of potential materials. Traditionally, design of new PV materials with appropriate properties is carried out using a simple trial-and-error approach, which is expensive and, more importantly, time-consuming. With the rapid development of high-speed computers and accumulation of data, the properties of PV materials can be predicted using algorithms based on a given set of examples. This is very exciting because these methods make it possible to predict fundamental properties of materials in an early stage of material design, even before the new material is synthesized, which could allow a very tailored synthetic route. Specific experiments can be designed and implemented to synthesize the corresponding materials according to the predictions. It has

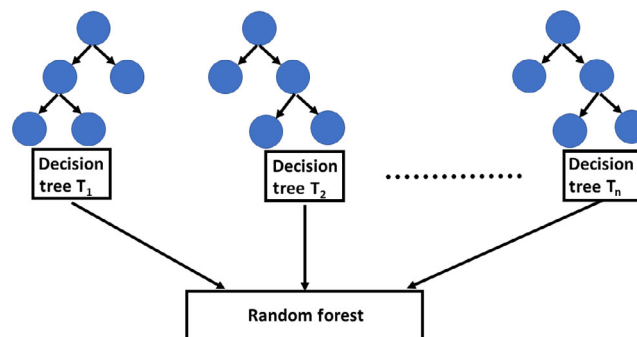


Figure 5. Structure of random forest algorithm.

Table 1. Summary of properties predicted by ML techniques.

Properties	ML techniques	References
Optical		
Absorption maxima	ANN, GA	[68,69]
Bandgap	RF, GA, SVM, KRR	[20,69–71,107]
Electrical		
Conductivity	ANN	[72]
Carrier mobility	ANN	[72]
Carrier density	ANN	[72]
Resistivity	ANN	[72]
Solubility	ANN	[74]
Stability	ERT + KRR, GA	[75,76]
I-V performance	kNN, RF, GA, GB	[19,77–83]
Spatial distance	GA	[69]
Reorganization energy	GA	[69]
Density surface	ANN	[84]
Tension viscosity	ANN	[84]

been demonstrated that ML techniques such as ANN and GA are efficient to predict the properties of PV materials. Most of the predictions in literatures are related to dye-sensitized solar cells (DSSCs) and organic solar cells (OSCs). **Table 1** summarizes the properties predicted by ML techniques.

3.1.1. Optical Properties

Jie Xu et al. predicted the absorption maxima of organic dyes for DSSCs using ANN.^[68] The reliability of the predictions was validated by the squared correlation coefficient (SCC), which is 0.991. Qingyou Zhang and Joao Aires-de-Sousa et al. introduced RF method into predicting the highest occupied and lowest unoccupied molecular orbitals (HOMO and LUMO) of organic materials.^[20] A mean absolute error (MAE) up to 0.15 eV and 0.16 eV was achieved for the HOMO and LUMO, respectively. In Ref.^[69] not only the HOMO and LUMO, but also other PV-related properties such as sunlight absorption, the spatial distance of the orbitals, and the reorganization energy of organic compounds have been successfully predicted using GA. In Ref.^[70] SVM was proposed to predict the bandgap of doped TiO₂. The predicted bandgap is in excellent agreement with the experimental results as reported in literatures. In Ref.^[71], Hongliang Xin et al. demonstrated that ML techniques such as KRR, SVM, and ANN could be applied to predict the energy gaps of more than 12 000 porphyrins with a reasonable root-mean-square error (RMSE) lower than 0.06 eV.

3.1.2. Electrical Properties

Based on ANN model, Sona Raeissi et al. predicted the temperature-dependent electrical conductivities of two ionic liquids made from 1-butyl-3-methylimidazolium hexafluorophosphate ([bmim][PF₆]) and [bmim][PF₆], respectively.^[72] By optimizing the structures of the ANN, a MSE of 2.87×10^{-8} and a SCC of 0.9981 were achieved. In

Ref.^[73], the electrical parameters such as majority carrier mobility, majority carrier density, and resistivity of multicrystalline (mc) solar grade silicon (SoG-Si) over a wide temperature range of 70–400 K and a specific range of compensation ratio were successfully predicted. The authors have shown that, compared with extensive simulated results, ANN can predict the three parameters with a maximum error of $\pm 10\%$.

3.1.3. Solubility

J. Darío Perea et al. used ANN to predict the solubility of organic semiconductors such as C₆₀, PC₆₁BM, bis-PC₆₁BM, ICMA, ICBA, and PC₇₁BM.^[74] The reliability of this method is demonstrated because of excellent agreement between the predicted results and the data obtained from the experiments. Also, the reliability of this method is proven due to a great match between the predicted results and those obtained from theoretical calculations such as molecular dynamics (MD) simulations and the functional group additive term (FGAT) method.

3.1.4. Stability

Whether a material can be synthesized and whether it could decompose under certain conditions depend on a key parameter, the thermodynamic phase stability. By combining ERT and KRR models, the stability of perovskite oxides was predicted in Ref.^[75] Results show that 11 out of 15 compounds are classified correctly with stable/unstable classifications. The prediction of completely new perovskites can be further improved if more information about the constituent elements is obtained and used in the training dataset. In Ref.^[76], previously unrecognized layered structure of two cuprous chalcogenides of Cu₂X (X = Te or Se) was predicted using GA. The newly discovered structure was found to be dynamically and mechanically stable. Also, the layered structure is predicted to be better than other structural forms at the interfaces of thin-film solar cells.

3.1.5. I-V Performances

In Ref.^[77], kNN method was applied to find appropriate oxides to fabricate single-junction solar cells from a large number of oxides consisting of TiO_x and CuO_x. With selection of appropriate material descriptors, virtual solar cells can be generated using kNN, which will predict the properties of materials. The results will help choose and manufacture materials, which can produce favorable PV properties. RF algorithm and GA were introduced in Ref.^[78] and Ref.^[79], respectively, into the design, synthesis, and characterization of a conjugated polymer for OSCs. It is demonstrated that if the processing parameters such as thickness, solvent, and thermal annealing were considered, reasonable prediction results could be achieved. In Ref.^[80], GA was used to predict the efficiencies of DSSCs made from five novel phenothiazine dyes. More than 9% efficiency can be obtained from these five dyes. Efficiencies of OSCs made from C60 derivatives were also predicted using GA in Ref.^[81]. The obtained results indicated the acceptable predictive ability of this method. I-V properties of new compounds could be predicted based on the results obtained from the predicted C60 derivatives, which will provide insights for designing new compounds with better properties. In^[82] the I-V parameters including open-circuit voltage

(V_{OC}), short-circuit current density (J_{SC}), fill factor (FF), and efficiency of CuInCdSSe thin-film solar cells were predicted using ANN with the material properties of CuInCdSSe thin film such as thickness, bandgap, crystallite size, dislocation density, micro-strain, activation energy, carrier concentration, and mobility, as inputs. Compared with experimentally obtained data, the mean squared error (MSE) of the predicted parameters is very small, indicating the proposed ANN can accurately predict the important parameters of the CuInCdSSe thin-film solar cells. In Ref.^[83], Mine Kaya and Shima Hajimirza applied ANN to predict the external quantum efficiency (EQE) of amorphous silicon (a-Si) thin-film solar cell. The inputs of the ANN are the thicknesses of each layer in the a-Si thin-film solar cell. The predicted EQE is close to that obtained from finite-difference time-domain (FDTD) simulations, and the overall computation time consumed by the ANN method is reduced by a factor of 5–20. In Ref.^[19], a range of ML techniques such as kNN, ANN, RF, and GB are applied to predict the efficiency of OSC. It was found that GB method could effectively predict the efficiency of OSC if the efficiency is in the range of 1%–9.5%. ANN method would be more preferable if the efficiency is outside the 1%–9.5% range.

3.1.6. Other Properties

In Ref.^[84], the density, surface tension, and viscosity of quaternary ammonium-based ionic liquids ($[N_{222(n)}]Tf_2N$ with $n = 5, 6, 8, 10, 12$) were predicted by ANN technique using the critical temperature, water content, and operation temperature as inputs. The results show that the selected parameters are very suitable for ANN to estimate the thermophysical properties of quaternary ammonium-based ionic liquids. Statistical results demonstrate that ANN is very effective on predicting the density, surface tension, and viscosity of new ionic liquids without reference to any experimental values.

Table 2. Summaries of the structures optimized by ML techniques.

Structures	ML techniques	References
Antireflection coating (ARC)	GA	[85,87,88]
	SA	[86]
	ACA	[65]
Light scattering	GA	[89–91,94,96,97]
	SA	[92,93]
	EA	[95,97,99]
	ANN	[98,100]
Doping profile	GA	[101,102,104]
	EA	[103]
Thickness	GA	[101,102,106,107]
	EA	[103]
	PSO	[105]
Front contact	GA	[104,109]
Morphology	PSO	[105]
Dimension of InAs/AlInAs Quantum well	GA	[108]
Device structure of perovskite/Si tandem solar cell	SA	[110]
	GA	[111]

3.2. Optimization of Device Structures

A typical PV device contains a couple of functional layers, which possess different properties. To improve the performance of solar cell, synergetic efforts are needed to optimize each layer in terms of different properties. It is almost impossible to consider so many parameters in a trial-and-error approach. However, with the aid of high-performance computers, ML techniques have been demonstrated to be able to efficiently optimize the structure of solar cells. **Table 2** summarizes the structures optimized by ML techniques.

3.2.1. Antireflection Coating (ARC)

In Ref.^[85], E. Schubert et al. applied GA technique to minimize the reflection of a multilayer ARCs made of TiO_2 and nanoporous SiO_2 . The thicknesses and compositions of individual layers were optimized. For Si solar cell, reflectivity is reduced by 31.1% if the fourth layer is added. An additional 5.6% reduction of reflectivity is achieved if the fifth layer is added. In Ref.^[86], Yin-Jung Chang and Yu-Ting Chen applied SA algorithm to optimize the structure of broadband omnidirectional ARCs for Si and $CuIn_{1-x}Ga_xSe_2$ (CIGS) solar cells. The refractive index and thickness of individual layers were optimized incorporating with solar spectrum. An average reflectance of 11.30% for wavelengths ranging from 400 nm to 1100 nm and incident angles from 0° to 80° were obtained using SiO_2/TiO_2 two-layer ARC for a metal-backed 300 μm c-Si. For 2 μm thick CIGS solar cell with a back reflector, an average reflectance of 8.46% for wavelengths ranging from 350 nm to 1200 nm and incident angles from 0° to 80° were achieved using single layer of MgF_2 . In Ref.^[65], similar optimization was implemented for Si solar cell using ACA method. The optimized three-layer ARC could provide an average reflectance of 2.98% over $\lambda = [400, 1100]$ nm for incident angles ranging from 0° to 80° and 6.56% for incident angles from 0° to 90° . In Ref.^[87], GA was used to optimize the structure of four-layer ARCs made of SiO_2 and TiO_2 for GaInP/GaAs/GaInAs triple-junction solar cell. Enhancement of 34.4% in the angle-of-incidence averaged J_{SC} was achieved. In Ref.^[88], the geometry of the periodic array of inverted pyramids and the thicknesses of the layers in crystal Si (c-Si) solar cells were optimized by GA. The results show that a J_{SC} of 37 $mA\ cm^{-2}$ can be achieved for a 40 μm thick c-Si when a-Si:H is used for the front-side passivation. The J_{SC} could be further increased to 39.1 $mA\ cm^{-2}$ if transparent AlO_x is used to passivate the front side of the solar cell.

3.2.2. Light Scattering

In Ref.^[89,90], the topology of a light-trapping structure was optimized based on GA method. The results have shown that the optimized light-trapping structure is highly efficient. More than threefold increase over the Yablonovitch limit and a broadband absorption efficiency of 48.1% have been obtained. In Ref.^[91], optical coupling and light trapping in a-Si thin-film solar cell were optimized to increase the quantum efficiency (QE). GA was applied to optimize the back reflector made of randomly textured ZnO/Ag. It was demonstrated that GA was very effective because a 29% improvement of quantum efficiency (QE) was obtained compared to flat cells, while a 9% improvement was achieved over the best periodic gratings. In Ref.^[92], SA algorithm was used to

optimize the structure of the micro-patterned OSC to enhance the light absorption. Up to 15% improvement in efficiency was obtained by patterning both the front and back electrodes with a periodic ridge shape, with conformally coated layers in-between, compared to the baseline configuration of a flat solar cell. In Ref.^[93], the morphology of two-dimensional nanotextured interface was optimized for thin-film Si solar cell to maximize the light scattering using SA algorithm. The J_{SC} can be increased from 14.3 mA cm^{-2} to 15.6 mA cm^{-2} . In Ref.^[94], the dimensions of the surface plasmon cavity in multijunction solar cells were optimized by GA method. For the optimized surface plasmon intermediate reflector and bottom-grating cavity, the long-wavelength absorption in the bottom cell was significantly increased by 63.27%, leading to an increase of 14.92% in the matched integrated absorbance. For the optimized surface plasma top- and bottom-grating cavity, the matched integrated absorbance was improved by 85.68% due to the higher transmission through front surface of the top solar cell and a more localized field in the bottom cell. In Ref.^[95], the EA technique was applied to optimize the dimensions of the two-level hierarchical nanostructure made of Ag nanoparticles in a-Si solar cells. The nanostructure can effectively scatter sunlight, leading to an increase of 10.23% in J_{SC} . In Ref.^[96], GA was applied to optimize the geometry of nanoantennas to maximize the light absorption in solar cells. It was found that the trunk conical antenna could increase the absorption by 21% compared with cylinder nanoantennas. In Ref.^[97], the effects of plasmon resonance were enhanced by addition of Ag hemispherical nanoparticles into CIGS thin film. The size and position of these Ag nanoparticles were optimized by GA and EA. The optimum obtained by GA method improved the efficiency of the solar cell but with a large consumption of Ag, while EA method could reduce the consumption of Ag by half and achieve almost the same efficiency as obtained with GA method. Similar optimization on the geometry of Ag sphere nanoparticles in P3HT:PCBM solar cell was implemented using ANN to maximize the absorption.^[98] It was found that absorption enhancement greater than 200% could be achieved. In Ref.^[99], EA method was applied to optimize the geometries of Ag and SiO_2 nanoparticles jointly placed in Si thin-film solar cell. In Ref.^[100], ANN was applied to optimize the device structure of P3HT:PCBM solar cell incorporated with Ag nanoparticles. A 325% of enhancement in absorption was obtained.

3.2.3. Doping Profile and Thickness

In Ref.^[101,102], the doping profile and thickness of each subcell in a quad junction solar cell of InGaP/GaAs/ InGaAs/Ge were optimized using GA. Compared with the original device, the efficiency of the optimized device was improved by 7.25%. In Ref.^[103], the doping profile and thickness of each layer in a-Si solar cell were optimized using EA method. The efficiency was significantly increased to 8.0% from the original efficiency of 5.68%. In Ref.^[104], the geometry of the front metal fingers and the doping profile of the emitter in c-Si solar cell were optimized using GA method. An optimal efficiency of 18.3% was obtained, which is in good agreement with similar results obtained for Si-based solar cell. This work shows the use of GA algorithms can be successfully used to optimize the geometrical parameters of solar cell. In Ref.^[105], PSO was proposed to optimize the thickness of active layer and morphology of the device in P3HT:PCBM solar cell. After 20 runs of the algorithm, it was found that the optimized value for domain size was 17 nm and the best thickness was 80 nm. The I-V properties of the solar cell were in well agreement with the experimental results

reported in literatures. In Ref.^[106], the thickness of the absorber, and the total recombination lifetime and mobility for electrons and holes in an intermediate band solar cell made from ZnTeO were optimized using GA. It has been found that an absolute gain of close to 1% in efficiency could be obtained by GA approach compared to analytical results as reported in literature. In Ref.^[107], GA was used to optimize the energy gaps and other relevant parameters such as impurity concentrations and the thicknesses of subcells in multijunction solar cell. More than 50% could possibly be obtained from quad junction solar cell under one sun.

3.2.4. Others

In Ref.^[108], Jelena Radovanovic et al. applied GA method to optimize the dimension of InAs/AlInAs quantum wells as an up-converter for Si solar cell. In Ref.^[109], the front metal grid of concentrated solar cell was optimized using GA technique. The efficiency was increased from 28.13% to 30.23% under 100 suns. In Ref.^[110], the device structure of monolithic planar perovskite/silicon tandem solar cell was optimized using SA algorithm. An absolute increase of 1.4 mA cm^{-2} in J_{SC} could be obtained for the optimized tandem solar cell, leading to an absolute gain of 2% in efficiency. An efficiency of 30.8% is achievable for this tandem cell if the bandgap of the perovskite is optimized. In Ref.^[111], the structure of the intermediate layer in perovskite/silicon tandem solar cells was optimized by GA in order to reduce the reflection losses

Table 3. Summaries of the fabrication processes optimized by ML techniques.

Processes	Materials	ML techniques	References
PECVD	Si_3N_4	ANN	[112–120]
		GA	[120]
co-firing	Ag grid	ANN + GA	[121–123]
		ANN + PSO	[122,123]
		ANN	[124]
Texturing	Si Wafer	ANN + GA	[125–128]
		ANN + PSO	[125–127]
Diffusion	Emitter	GA	[129,130]
		ANN + GA	[125–127]
		ANN + PSO	[125–127]
Deposition	TiO_2	GA	[131,132]
		ANN	[133]
Laser scribing	AZO	ANN	[134]
Deposition	CIGS	RF	[135]
Doping	Mn in CZTSSe	SEK	[61]
Deposition	Perovskite	GA	[136]
Annealing	P3HT:PCBM	DT	[62]
		SVM	[62]
Loading	Dye	ANN + GA	[137]
Defective area removal	Si wafer	FL	[63]
Cutting	Si wafer	ANN	[138]
Lapping	Si wafer	ANN	[139,140]

caused by the charge selective contacts between the top cell and the bottom cell. The tandem solar cell incorporated with the optimized inter-layer shows an absolute enhancement 0.82 mA cm^{-2} in J_{SC} .

3.3. Optimization of Fabrication Processes

It is extremely difficult to determine the exact relationship between the desired properties of PV materials and the controllable fabrication conditions due to wide range of processing parameters and trade-off among different properties. ML techniques can create models, which can be effectively trained using available data, and precisely predict the properties of materials in an unexplored chemical space, which can then be specifically designed and synthesized. ML techniques have been applied to optimize the fabrication processes for Si_3N_4 thin film, metal contact, texturing, and emitter in Si solar cell, TiO_2 photoanode in DSSC, laser scribing in thin-film solar cell, deposition of thin-film absorber layer, and processing of Si wafer. Cost and time in the experimental designs have been significantly reduced. **Table 3** summarizes the fabrication processes optimized by ML techniques.

3.3.1. Plasma-Enhanced Chemical Vapor Deposition (PECVD) of Si_3N_4 Thin Films

In Ref.^[112–116], experimental results on the PECVD of Si_3N_4 thin films were used to train the ANN model, which then accurately revealed the effects of deposition conditions on film properties. It was found that the process parameters such as temperature, SiH_4 , and NH_3 flow rate are crucial to increase the hydrogenation and therefore to enhance the carrier lifetime in polysilicon solar cells. In Ref.^[117,118], ANN was applied to examine the effect of the interaction among the process parameters on the refractive index. It was found that the SiH_4 flow rate was the most influential variable. Many interaction effects unnoticed previously were illustrated and reasonably interpreted with respect to the SiH/NH bond ratio. As a result, the ANN model of the refractive index greatly facilitated not only understanding of deposition mechanisms, but also for finding useful trade-offs between the variables. In Ref.^[119], a room temperature PECVD process was optimized using ANN to obtain a relatively high deposition rate by controlling the duty ratio and bias power. The lack of N atoms available to Si-Si on the film surface was revealed to be the primary cause lowering the deposition rate at lower duty ratio. In Ref.^[120], a method combining ANN and GA was proposed to optimize the process parameters in PECVD Si_3N_4 thin films such as power, pressure, SiH_4 flow rate, NH_3 flow rate, N_2 flow rate, and substrate temperature. Compared to conventional and statistical regression methods, this method achieved an improvement of 73% and 81% in carrier lifetime, respectively.

3.3.2. Contact Formation

In Ref.^[121], ANN and GA were combined to optimize the co-firing process conditions of a screen-printed Ag grid on the front surface and Al on the back surface of monocrystal Si solar cell. The success of this method was demonstrated by additional experiments, which obtained an average efficiency of 15.44%. Compared to the previous experiments implemented using design of experiment (DOE), the efficiency

was improved by 3.9%. In Ref.^[122,123], ANN was combined with GA and PSO, respectively, to optimize the co-firing process parameters including the temperatures of each of three zones in the belt furnace and the belt speed. It was found that the optimized efficiency by PSO was slightly higher than that determined by GA. More importantly, repeated applications of PSO generated process parameters with smaller standard deviations, indicating better consistency in process parameter production. In Ref.^[124], ANN method was applied to minimize the contact resistance between the front electrode and the Si. The process parameters including paste composition, morphology of the silicon substrate, co-firing temperature, the power of the laser beam, and the scanning speed of the laser beam in the co-firing and selective laser sintering process were optimized.

3.3.3. Texturing and Emitter Formation

In Ref.^[125–127], fabrication process conditions of Si solar cell such as texturing time, amount of N_2 , DI water, diffusion time, and temperature were optimized using ANN in combination with GA and PSO, respectively. The amount of N_2 , DI water, and diffusion time optimized by the two approaches was considerably different. Furthermore, repeated applications of PSO generated process parameters with smaller standard deviations, indicating better consistency in process parameter production. In Ref.^[128], the reagent ratio and reaction time in the acidic texturing process of mc-Si wafer were optimized by ANN in combination with GA. The best recipe was found to be $\text{HF}:\text{HNO}_3:\text{NaH}_2\text{PO}_4\cdot 2\text{H}_2\text{O} = 9:1:7$. A reflectance of 17% and a texturing speed close to $2 \mu\text{m min}^{-1}$ were achieved with a texturing appropriate for mass production. In Ref.^[129], the diffusion process parameters such as POCl_3 flow, O_2 flow, N_2 flow, and process time were optimized by GA method. An expected sheet resistance with high uniformity was achieved. In Ref.^[130], the process parameters in phosphorous diffusion were optimized by GA. The results indicate that a high temperature step followed by a low temperature step or a slow annealing step helps to reduce the impact of iron impurities, leading to a higher carrier lifetime, which was confirmed by the experiments.

3.3.4. TiO_2 Photoanode in DSSC

In Ref.^[131], GA method was applied to optimize the photoanodes in DSSC composing of various sizes of TiO_2 nanoparticles and multiwalled carbon nanotubes in a double-layer configuration. A best efficiency of 7.3%, which was the highest efficiency then reported on DSSC made from TiO_2 films without post-treatment, was achieved after 3 generations. In Ref.^[132], GA method was applied to optimize the photoanodes in DSSC made of TiO_2 nanoparticles with different sizes and dye loadings. DSSC made from the photoanode consisting of a mixture of TiO_2 nanoparticles with sizes of 14, 21, and 40 nm, and with different dye loadings, compressed to a thickness of 8 μm under 94 MPa, achieved the highest efficiency of 6.02%, which was 22% higher than that reported previously without the assistance of GA.

In Ref.^[133], ANN was applied to investigate the effects of deposition process parameters, such as withdrawal velocity, drying temperature, and number of deposited layers, on the growth rate of TiO_2 -nanostructured thin film prepared with the sol-gel dip-coating method. The

results show that the proposed ANN method can reasonably estimate the effects of the parameters.

3.3.5. Laser Scribing

In Ref.^[134], ANN was used to optimize the laser scribing process of ZnO:Al (AZO) thin film. The process parameters optimized were repetition rate, laser power, scanning speed, start delay, corner delay, displacement delay, start angle, and focusing position. The optimal conditions were 65 kHz, 9.84 W, 100 mm s⁻¹, 0 ms, 2 ms, 6 ms, 1 mdeg, and 30 106 µm, respectively. Predictive results by ANN approach were found to be better than other conventional approach. The reliability of this approach was confirmed by experiments.

3.3.6. Deposition of Thin-Film Absorber Layer

In Ref.^[135], RF algorithm was applied to analyze the process parameters of the 3-stage CIGS solar cell, in order to reveal the most relevant for the I-V performance. The analyzed parameters include stage duration times, heater power values, temperatures for the element sources, and the temperature of the substrate. It was found that the most relevant variable was the 2nd-stage duration time, which is in well agreement with the experimental knowledge. In Ref.^[61], squared-exponential kernel (SEK) method was applied to optimize the doping of Mn in Cu₂ZnSn(S,Se)₄ (CZTSSe) solar cells. With the assistance of this method, the optimal doping concentration of Mn in CZTSSe thin film was rapidly and efficiently found, resulting in a highest efficiency of 8.9% in experiment. In Ref.^[136], the dipping time and spin speed in deposition of perovskite thin film were optimized using GA method. A maximum efficiency of 8.75% was obtained. This method is very efficient in optimizing the processes because there were totally only 18 samples fabricated even though two parameters with 12 levels were considered, which conventionally requires 2^[12] samples to be fabricated. In Ref.^[62], ML techniques such as DT and SVM were successfully applied to map the domain sizes in P3HT:PCBM blended thin films to their annealing temperatures. This is significant because the optimized domain sizes obtained through simulation could now be converted to actual annealing temperature in device fabrication. In Ref.^[137], the dye loading process was optimized by ANN combined with GA to improve the efficiency and the durability of DSSC. The optimized parameters were volume ratio of organic dyes, concentration of anti-aggregation agent, and manufacture temperature. The best parameters were found by this method and applied in fabricating the solar cells. An exceptional agreement between the optimization and the experiment was achieved.

3.3.7. Processing of Si Wafer

In Ref.^[63], FL algorithm was applied to optimize the cutting path of Si wafers. Results show that defective areas in the wafer can be cut and removed along the path, preserving greater usable area compared to the traditional cutting method. In Ref.^[138], the process parameters in diamond wire saw cutting such as spool speed, z-axis speed, and oil ratio in a coolant slurry were optimized by ANN. The surface roughness

Table 4. Summaries of the measurement data reconstructed by ML techniques.

Original data	ML techniques	Final results	References
EL images	AB	Surface crack	[64]
	SVM	Micro-crack	[141,142]
STEM	VCA	Defective region	[143]
Diffraction pattern	ANN	Morphology and structure	[144]
EDX	NNMF	Degradation	[66]
Transmittance	GA, PSO	Optical constants	[145,146]
	GA, PSO	Thickness	[145,146]
LIBS	ANN	Layers in CIGS	[147,148]
LLRPI	ANN	Chemical stain	[149]

values of Si wafer were minimized. In Ref.^[139,140], the process parameters in lapping such as rotation speed, lapping duration, and lapping pressure were optimized by ANN. Results obtained from ANN method were validated with a success over 99%.

3.4. Reconstruction of Measurement Data

The properties of PV materials and devices usually can be obtained directly using certain characterization techniques. However, in some cases, the data obtained need to be further processed to more accurately evaluate the properties of PV materials and devices. A few ML techniques have been applied to reconstruct the measurement data in literatures. **Table 4** summarizes the measurement data reconstructed by ML techniques.

3.4.1. Electroluminescence (EL) Images

In Ref.^[64], Li Bin et al. applied AB algorithm to process the electroluminescence images obtained from Si solar cells to detect the surface crack. The experimental results show that this technique can efficiently, robustly, and automatically inspect the surface crack in Si solar cells. In Ref.^[141,142], SVM algorithm was used to process the electroluminescence images obtained from multi-Si solar cells to detect the surface crack. Results indicate that the methods and procedures can accurately detect micro-crack in solar cells with sensitivity, specificity, and accuracy averaging at 97%, 80%, and 88%, respectively.

3.4.2. Electron Microscopy

In Ref.^[143], M. Duchamp et al. applied a vortex component analysis (VCA) algorithm to process the scanning transmission electron microscopy (STEM) spectrum obtained from hydrogenated micro-crystalline Si (µc-Si:H) solar cell. The results show that the defective regions located close to the front contact are primarily empty. The deposited ZnO can fill into the defective region during deposition of the top contact of the solar cell. In Ref.^[144], ANN was applied to analyze the laser-induced diffraction pattern of CdTe thin films to obtain the morphological and structural properties. The results are very consistent with what have been found by conventional microscopic techniques such as scanning electron microscopy (SEM) and

transmission electron microscopy (TEM). In Ref.^[66], NNMF method was used to process the measurement data obtained by scanning transmission electron microscopy (STEM) and energy-dispersive X-ray spectroscopy (EDX). Different nanometer-scale processes, which contribute to the degradation of perovskite solar cell, have been identified. It was found that the migration of iodine into the hole transport layer, spiro-OMeTAD, toward the gold electrode resulted in a severe degradation of the perovskite solar cell.

3.4.3. Transmittance

In Ref.^[145], Zhiqiang Gao et al. applied GA method to the transmittance spectrum obtained from blended organic thin film consisting of CuPc and C60. The extinction coefficient, refractive index, and thickness of the blended thin film can be accurately derived. In Ref.^[146], Yuan Yuan et al. applied PSO algorithm to process the transmittance of optical thin film. The optical constants and thickness of the thin film obtained by this method were in well agreement with those reported in literature. The effectiveness and the feasibility of the PSO method deriving the optical constants are verified.

3.4.4. Laser-Induced Breakdown Spectroscopy (LIBS)

In Ref.^[147,148], ANN was applied to reconstruct the LIBS obtained from CIGS solar cell during the P1, P2, and P3 processes. Transitions between layers during laser scribing can be accurately identified with low error, high sensitivity, high precision, and high specificity. If the classification method can be customized for each processing step, better performance can be achieved.

3.4.5. Laser Light Reflection Point Images (LLRPI)

In Ref.^[149], ANN method was proposed to assist the analysis of LLRPI obtained from polycrystal Si wafers to detect chemical stains. The validity of the proposed method has been demonstrated because it has achieved a recognition rate of 98% for more than 1 000 images.

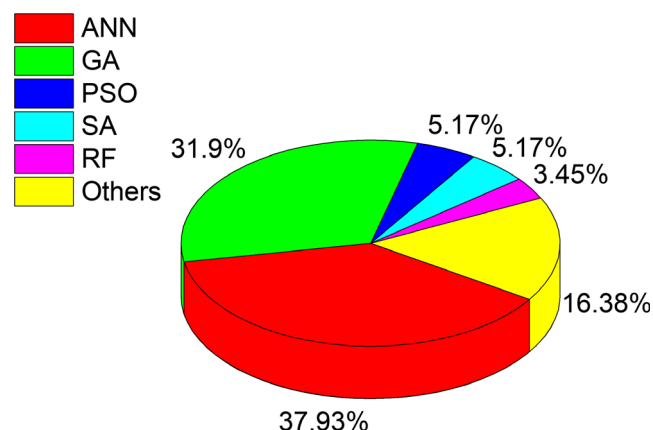


Figure 6. Distribution of types of ML techniques applied in design and fabrication of solar cells.

4. Trends of ML Techniques in Solar Cell

To track the trends of ML techniques applied in the design and fabrication of solar cell, the literatures over the last 12 years are quantitative analyzed. The results shown in this article do not represent the exact number of literatures covering ML techniques in solar cells, but approximate trends can be observed. As shown in **Figure 6**, ANN and GA are the two most applied ML techniques. ANN models require less formal statistical training to develop. By modeling of ANN, the nonlinear relationship can be detected implicitly between independent and dependent variables. Moreover, different training algorithms can be selected to develop ANN model for different scenarios. Similarly, GA does not involve sophisticated mathematical techniques. It is easy to be handled by interested researchers. It only involves stochastic search techniques based on natural genetics and natural selection. Meanwhile, the evolution operators of GA can be effectively applied to perform global search. GA has a great flexibility to be combined with other algorithm to produce an efficient hybrid model for some specific scenarios. The distribution of applications in design and fabrication of solar cells assisted by ML techniques is shown in **Figure 7**. ML techniques have been mostly applied in optimization of device structures and optimization of fabrication processes, indicating ML techniques are more suitable for these two applications.

Figure 8 shows the cumulative number of ML techniques applied in design and fabrication of solar cells. The ML techniques had been rarely applied in design and fabrication of solar cells before 2006. This is partly due to the lack of interest in PV technologies before 2006. The PV technologies have been significantly improved due to the generous financial support from governments since 2006, resulting in widespread installation of PV systems worldwide and different PV technologies being developed. With the rapid development of artificial intelligence, its effectiveness has been widely recognized. The application of ML techniques in the design and fabrication of solar cells started slowly but has recently gained tremendous momentum as observed in **Figure 8**.

5. Conclusions

This article presents a comprehensive review of the design and fabrication of solar cells assisted by ML techniques. ML techniques are proven

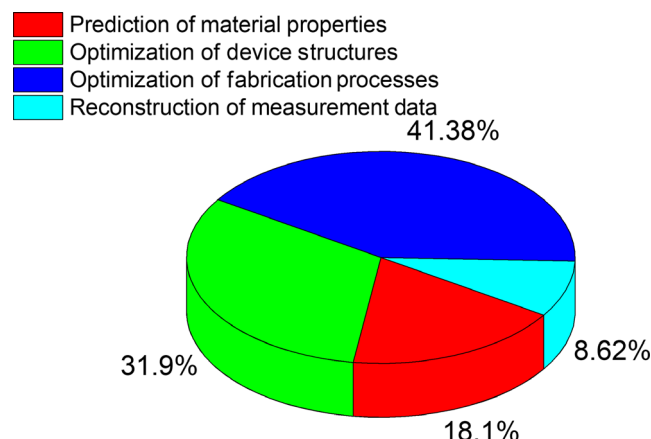


Figure 7. Distribution of applications in design and fabrication of solar cells assisted by ML techniques.

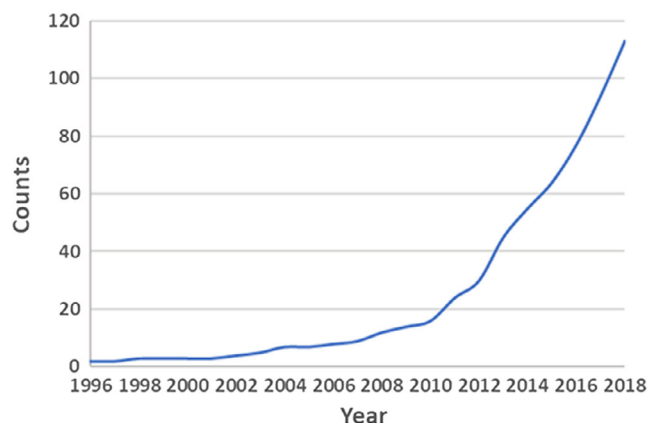


Figure 8. Cumulative number of ML techniques applied in design and fabrication of solar cells.

to be very effective in assisting the design and fabrication of solar cells when data are properly collected. The application of ML techniques not only reduces the cost and time, but also sometimes can lead to better properties and higher performances. If combined with other tools and fed with additional theoretical and experimental data, more accurate and robust results can be achieved from ML techniques. An exhaustive search and compilation of the literatures indicate that all the major aspects in the research and development of solar cells can be effectively assisted by ML techniques. The aspects have been grouped into four categories:

- **Prediction of material properties** Material properties including optical, electrical, and other physical properties such as solubility, spatial distance, reorganization energy, density, surface tension, and viscosity can be efficiently predicted. The I-V properties such as efficiency and EQE of solar cells made of a wide range of PV materials can also be accurately predicted.
- **Optimization of device structures** A wide range of device structure-related aspects including ARC, light scattering, doping profile, thickness, front contact, morphology, dimension of InAs/AlInAs quantum well, and the geometry of the subcells in perovskite/Si tandem solar cell have been optimized by ML techniques. A typical PV device contains a couple of functional layers, which possess different properties. ML techniques make it possible to consider the synergetic effects of these properties in improving the performance of solar cells.
- **Optimization of fabrication processes** ML techniques have been proven to be effective in optimizing the fabrication processes such as PECVD, co-firing, texturing, diffusion, deposition, laser scribing, doping, annealing, dye loading, defective area removal, cutting, and lapping. Most of the fabrication processes involving ML techniques are related to Si solar cell, while only a few literatures reported the application of ML techniques in optimizing the fabrication processes related to other PV technologies such as CIGS, CdTe, DSSC, and OSC. ML techniques can effectively model the correlation between the properties of the PV materials and the corresponding fabrication methods if they are trained using sufficient experimental data.
- **Reconstruction of measurement data** ML techniques have been demonstrated to be effective to process the measurement data obtained

using EL images, STEM, diffraction pattern, EDX, transmittance, LIBS, and LLRPI. The properties of PV materials and devices which are otherwise difficult to be explored without complex measurement tools can now be conveniently obtained using regular characterization techniques.

An illustrative statistical analysis of the literatures indicating the current state and the future trends of the ML techniques applied in the design and fabrication of solar cells has also been presented in this article. ANN and GA are the two most applied ML techniques because the application of these two ML techniques does not necessarily involve sophisticated mathematical techniques. Topics in the optimization of device structures and optimization of fabrication processes are more popular in terms of ML techniques. The application of ML techniques in the design and fabrication of solar cells started slowly but has gained tremendous momentum recently. This article can be used as a reference by all PV researchers who are interested in ML techniques. With collective efforts among research institutions, industries, investors, and governments, scientific data obtained from experiments and theoretical calculations will be timely reported and widely disseminated. Although ML techniques have not yielded tremendous achievement in terms of conversion efficiency of solar cells, further advancement will surely contribute toward cost-effective development of solar cells, especially for the discovery of suitable PV materials.

Acknowledgement

The work reported here has been partially supported by Nanchang University, under Research Grant 9166-2701010119.

Conflict of Interest

The authors declare no conflict of interest.

Keywords

design and fabrication, machine learning, optimization, solar cell

Received: August 8, 2019

Revised: September 12, 2019

- [1] F. Almonacid, E. F. Fernandez, A. Mellit, S. Kalogirou, *Renew Sust Energ Rev* **2017**, 75, 938.
- [2] L. C. Andreani, A. Bozzola, P. Kowalczewski, M. Liscidini, L. Redorici, *Adv Phys-X* **2018**, 4, 1548305.
- [3] J. P. Correa-Baena, A. Abate, M. Saliba, W. Tress, T. J. Jacobsson, M. Gratzel, A. Hagfeldt, *Energ Environ Sci* **2017**, 10, 710.
- [4] J. Ramanujam, U. P. Singh, *Energ Environ Sci* **2017**, 10, 1306.
- [5] Y. Liu, S. Wang, L. M. Peng, *Adv Energy Mater* **2016**, 6, 1600522.
- [6] L. F. Wang, F. J. Si, F. L. Tang, H. T. Xue, *Mater Res Express* **2019**, 6, 026312.
- [7] L. H. Li, J. L. Mi, Y. C. Yong, B. D. Mao, W. D. Shi, *J Mater Chem C* **2018**, 6, 8226.
- [8] N. Hernandez-Haro, J. Ortega-Castro, Y. B. Martynov, R. G. Nazmitdinov, A. Frontera, *Chem Phys* **2019**, 516, 225.
- [9] P. Pounraj, V. Mohankumar, M. S. Pandian, P. Ramasamy, *J Mol Model* **2018**, 24, 343.

- [10] A. Ruth, M. C. Brennan, S. Draguta, Y. V. Morozov, M. Zhukovskiy, B. Janko, P. Zapol, M. Kuno, *Acs Energy Lett* **2018**, 3, 2321.
- [11] L. Sousa, R. Volpi, D. A. da Silva Filho, M. Linares, *Chem Phys Lett* **2017**, 689, 74.
- [12] U. Neupane, B. Bahrami, M. Biesecker, M. F. Baroughi, Q. Q. Qiao, *Nano Energy* **2017**, 35, 128.
- [13] B. J. Ainscough, E. K. Barnell, P. Ronning, K. M. Campbell, A. H. Wagner, T. A. Fehniger, G. P. Dunn, R. Uppaluri, R. Govindan, T. E. Rohan, M. Griffith, E. R. Mardis, S. J. Swamidass, O. L. Griffith, *Nat Genet* **2018**, 50, 1735.
- [14] F. Y. Dao, H. Lv, F. Wang, H. Ding, *Front Genet* **2018**, 9, 613.
- [15] J. L. Fan, L. F. Wu, F. C. Zhang, H. J. Cai, W. Z. Zeng, X. K. Wang, H. Y. Zou, *Renew Sust Energy Rev* **2019**, 100, 186.
- [16] R. Zhao, R. Q. Yan, Z. H. Chen, K. Z. Mao, P. Wang, R. X. Gao, *Mech Syst Signal Pr* **2019**, 115, 213.
- [17] J. E. Villanueva-Meyer, P. Chang, J. M. Lupo, C. P. Hess, A. E. Flanders, M. Kohli, *Am J Roentgenol* **2019**, 212, 52.
- [18] J. Q. Lv, Z. Y. Na, X. Liu, Z. Deng, *Comm Signal Process Syst* **2019**, 463, 2429.
- [19] H. Sahu, W. Rao, A. Troisi, H. Ma, *Adv Energy Mater* **2018**, 8, 1801032.
- [20] F. Pereira, K. X. Xiao, D. A. R. S. Latino, C. C. Wu, Q. Y. Zhang, J. Aires-de-Sousa, *J Chem Inf Model* **2017**, 57, 11.
- [21] L. C. Rabelo, X. J. R. Avula, *Int J Prod Res* **1992**, 30, 315.
- [22] H. S. Green, T. Triffet, *Math Comput Model* **1993**, 18, 1.
- [23] I. E. Dror, F. L. Florer, D. Rios, M. Zagaeski, *Biol Cybern* **1996**, 74, 331.
- [24] A. Greco, N. Mammone, F. C. Morabito, M. Versaci, Presented in part at the Enformatika, Vol 7: lec 2005 Proceedings, **2005**.
- [25] Z. Khan, A. E. K. Lim, L. I. Wang, X. G. Wang, R. Beltran, *Text Res J* **2009**, 79, 714.
- [26] J. M. Johns, D. Burkes, *J Nucl Mater* **2017**, 490, 155.
- [27] S. Srinivasan, T. Kamalakannan, *Comput Econ* **2018**, 52, 443.
- [28] A. Sahu, S. K. Pradhan, *Mater Today-Proc* **2018**, 5, 25075.
- [29] S. Kumar, S. Singh, J. Kumar, *Wireless Pers Commun* **2018**, 103, 2435.
- [30] R. C. Lv, L. Y. Xiao, X. Jiang, M. Feng, F. Yang, J. Tian, *Acs Biomater Sci Eng* **2018**, 4, 4378.
- [31] B. Gao, X. Q. Li, W. L. Woo, G. Y. Tian, *Ieee T Image Process* **2018**, 27, 2160.
- [32] Y. N. Zhang, Y. H. Zhou, *J Netw Comput Appl* **2018**, 119, 110.
- [33] T. T. Yu, W. Srisa-an, M. B. Cohen, G. Rothermel, *Softw Test Verif Rel* **2018**, 28, e1686.
- [34] R. Vijayanand, D. Devaraj, B. Kannapiran, *Comput Secur* **2018**, 77, 304.
- [35] Z. Y. Jia, J. Q. Yu, X. L. Ai, X. Xu, D. Yang, *Aerosp Sci Technol* **2018**, 76, 112.
- [36] H. M. Jiang, C. K. Kwong, W. Y. Park, K. M. Yu, *J Eng Design* **2018**, 29, 381.
- [37] N. Lynn, M. Z. Ali, P. N. Suganthan, *Swarm Evol Comput* **2018**, 39, 24.
- [38] A. Otto, N. Agatz, J. Campbell, B. Golden, E. Pesch, *Networks* **2018**, 72, 411.
- [39] Z. Q. Wang, X. Sun, D. X. Zhang, *Bio-Inspired Comput Intelligence Appl* **2007**, 4688, 307.
- [40] N. Tian, J. Sun, W. B. Xu, C. H. Lai, *Inverse Probl Sci En* **2011**, 19, 181.
- [41] L. Q. Yang, Y. Zheng, Y. Z. Xu, Y. J. Bai, 2017 International Conference on Computer Systems, Electronics and Control (Iccsec), **2017**, 1262.
- [42] J. Branke, S. Meisel, C. Schmidt, *J Heuristics* **2008**, 14, 627.
- [43] L. L. Laudis, S. Anand, A. K. Sinha, Presented in part at the 2015 International Conferenced on Circuits, Power and Computing Technologies (Iccpct-2015), **2015**.
- [44] M. G. Nejad, H. Guden, B. Vizvari, R. V. Barenji, *Adv Mech Eng* **2018**, 10, 1687814017753912.
- [45] J. Sousa, J. Muranho, A. S. Marques, R. Gomes, *J Water Res Plan Man* **2016**, 142, C4015010.
- [46] M. L. D. Dias, A. R. R. Neto, *Expert Syst Appl* **2017**, 87, 157.
- [47] V. N. Ikonomidou, P. van Gelderen, J. A. de Zwart, M. Fukunaga, J. H. Duyn, *Magnet Reson Med* **2005**, 54, 373.
- [48] T. D. Martins, E. D. L. B. de Camargo, R. G. Lima, M. B. P. Amato, M. D. G. Tsuzuki, *Ieee T Bio-Med Eng* **1861**, 2012, 59.
- [49] C. Li, Y. Tao, W. G. Ao, S. Yang, Y. Bai, *Energy* **2018**, 165, 1220.
- [50] S. P. Chatzis, V. Siakoulis, A. Petropoulos, E. Stavroulakis, N. Vlachogiannakis, *Expert Syst Appl* **2018**, 112, 353.
- [51] K. Doubleday, H. Zhou, H. D. Fu, J. Zhou, *J Comput Graph Stat* **2018**, 27, 849.
- [52] F. Rahimian, G. Salimi-Khorshidi, A. H. Payberah, J. Tran, R. A. Solares, F. Raimondi, M. Nazarzadeh, D. Canoy, K. Rahimi, *PLoS Medicine* **2018**, 15, e1002695.
- [53] C. Beeler, L. Dbeibo, K. Kelley, L. Thatcher, D. Webb, A. Bah, P. Monahan, N. R. Fowler, S. Nicol, A. Judy-Malcolm, J. Azar, *Am J Infect Control* **2018**, 46, 986.
- [54] W. X. Yao, C. X. Zhang, H. D. Hao, X. Wang, X. L. Li, *Renew Energy* **2018**, 128, 155.
- [55] J. Naik, R. Bisoi, P. K. Dash, *Renew Energy* **2018**, 129, 357.
- [56] H. Guo, J. Y. Zhao, X. N. Li, *Int J Mater Prod Tec* **2019**, 58, 1.
- [57] A. Celisse, T. Mary-Huard, *J Mach Learn Res* **2018**, 19, 2373.
- [58] D. P. Xiong, Q. L. Gui, W. G. Hou, M. Y. Ding, *Inform Sci* **2018**, 454, 328.
- [59] J. Luan, Z. Yao, F. T. Zhao, X. Song, *Math Comput Simulat* **2019**, 156, 294.
- [60] X. Zhang, J. G. Luo, X. M. Sun, J. C. Xie, *Eng Optimiz* **2019**, 51, 42.
- [61] X. Li, Z. Hou, S. Gao, Y. Zeng, J. Ao, Z. Zhou, B. Da, W. Liu, Y. Sun, Y. Zhang, *Solar RRL* **2018**, 2, 1800198.
- [62] F. Lan, M. L. Jiang, F. N. Wei, Q. Tao, G. Y. Li, Presented in part at the 2016 Ieee 16th International Conference on Nanotechnology (Ieee-Nano), **2016**.
- [63] C. J. Lin, Y. J. Shiue, M. T. Su, C. Y. Lee, *Indian J Eng Mater S* **2013**, 20, 213.
- [64] B. Li, X. H. He, S. Fang, *Chin Cont Decis Conf* **2011**, 993.
- [65] X. Guo, H. Y. Zhou, S. Guo, X. X. Luan, W. K. Cui, Y. F. Ma, L. Shi, *Opt Express* **2014**, 22, A1137.
- [66] S. Cacovich, G. Divitini, C. Ireland, F. Matteocci, A. Di Carlo, C. Ducati, *Chemsuschem* **2016**, 9, 2673.
- [67] A. Youssef, M. El-Telbany, A. Zekry, *Renew Sust Energy Rev* **2017**, 78, 72.
- [68] J. Xu, H. Zhang, L. Wang, G. J. Liang, L. X. Wang, X. L. Shen, *Mol Simulat* **2011**, 37, 1.
- [69] K. Huwig, C. C. Fan, M. Springborg, *J Chem Phys* **2017**, 147, 234105.
- [70] T. O. Owolabi, K. O. Akande, S. O. Olatunji, N. Aldhafferi, A. Alqah-tani, *Aip Adv* **2017**, 7, 115225.
- [71] Z. Li, N. Omidvar, W. S. Chin, E. Robb, A. Morris, L. Achenie, H. L. Xin, *J Phys Chem A* **2018**, 122, 4571.
- [72] A. Z. Hezave, M. Lashkarbolooki, S. Raeissi, *Fluid Phase Equilib* **2012**, 314, 128.
- [73] J. C. Patra, C. Modanese, M. Acciarri, *Iet Renew Power Gen* **2016**, 10, 1010.
- [74] J. D. Perea, S. Langner, M. Salvador, J. Kontos, G. Jarvas, F. Winkler, F. Machui, A. Gorling, A. Dallos, T. Ameri, C. J. Brabec, *J Phys Chem B* **2016**, 120, 4431.
- [75] D. Han, T. Zhang, M. L. Huang, D. Y. Sun, M. H. Du, S. Y. Chen, *Appl Mater* **2018**, 6, 084902.
- [76] M. C. Nguyen, J.-H. Choi, X. Zhao, C.-Z. Wang, Z. Zhang, K.-M. Ho, *Phys Rev Lett* **2013**, 111, 165502.
- [77] A. Yosipof, O. E. Nahum, A. Y. Anderson, H. N. Barad, A. Zaban, H. Senderowitz, *Mol Inform* **2015**, 34, 367.
- [78] S. Nagasawa, E. Al-Naamani, A. Saeki, *J Phys Chem Lett* **2018**, 9, 2639.
- [79] N. M. O'Boyle, C. M. Campbell, G. R. Hutchison, *J Phys Chem C* **2011**, 115, 16200.
- [80] V. Venkatraman, M. Foscatto, V. R. Jensen, B. K. Alsberg, *J Mater Chem A* **2015**, 3, 9851.
- [81] E. Pourbasheer, A. Banaei, R. Aalizadeh, M. R. Ganjali, P. Norouzi, J. Shadmanesh, C. Methenitis, *J Ind Eng Chem* **2015**, 21, 1058.
- [82] K. V. Khot, T. D. Dongale, S. S. Mali, C. K. Hong, R. K. Kamat, P. N. Bhosale, *J Mater Sci* **2017**, 52, 9709.

- [83] M. Kaya, S. Hajimirza, *Sci Rep-Uk* **2018**, 8, 8170.
- [84] K. Golzar, S. Amjad-Iranagh, H. Modarress, J. Disper, *Sci Technol* **2014**, 35, 1809.
- [85] M. F. Schubert, F. W. Mont, S. Chhajer, D. J. Poxson, J. K. Kim, E. F. Schubert, *Opt Express* **2008**, 16, 5290.
- [86] Y. J. Chang, Y. T. Chen, *Opt Express* **2011**, 19, A875.
- [87] X. Yan, D. J. Poxson, J. Cho, R. E. Welser, A. K. Sood, J. K. Kim, E. F. Schubert, *Adv Funct Mater* **2013**, 23, 583.
- [88] A. Mayer, J. Muller, A. Herman, O. Deparis, *Active Photonic Materials VII* **2015**, 9546, 95461N.
- [89] C. Wang, S. C. Yu, W. Chen, C. Sun, *Sci Rep-Uk* **2013**, 3, 1025.
- [90] C. Wang, S. C. Yu, W. Chen, C. Sun, *Thin Film Solar Technol V* **2013**, 8823, 88230C.
- [91] A. Lin, J. Phillips, *Sol Energ Mat Sol C* **2008**, 92, 1689.
- [92] C. Kirsch, S. Mitran, *J Appl Phys* **2012**, 112, 054502.
- [93] K. Jager, M. Fischer, R. A. C. M. M. van Swaaij, M. Zeman, *Opt Express* **2013**, 21, A656.
- [94] A. S. Lin, S. M. Fu, Y. K. Zhong, C. W. Tseng, S. Y. Lai, T. C. K. Lau, *Opt Eng* **2013**, 52, 064002.
- [95] S. W. Zhou, X. D. Hunang, Q. Li, Y. M. Xie, *Opt Express* **2013**, 21, A285.
- [96] M. L. C. da Silva, V. Dmitriev, K. Q. da Costa, Presented in part at the 2015 Sbmo/leee Mtt-S International Microwave and Optoelectronics Conference (Imoc), **2015**
- [97] G. Aiello, S. Alfonzetti, S. A. Rizzo, N. Salerno, *leee T Magn* **2015**, 51, 1.
- [98] M. Kaya, S. Hajimirza, *Energies* **1981**, 2017, 10.
- [99] G. Aiello, S. Alfonzetti, S. A. Rizzo, N. Salerno, *Energies* **2017**, 10, 53.
- [100] M. Kaya, S. Hajimirza, *Sol Energy* **2018**, 165, 159.
- [101] S. Michael, D. Bates, J. Utsler. Conference Record of the 2006 leee 4th World Conference on Photovoltaic Energy Conversion, 1 and 2, **2006**, 1834.
- [102] D. J. Poxson, M. F. Schubert, F. W. Mont, E. F. Schubert, J. K. Kim, *Opt Lett* **2009**, 34, 728.
- [103] Y. M. Li, Y. Y. Chen, C. Y. Chen, C. H. Shen, H. W. Cheng, I. H. Lo, C. N. Chen, *Mater Manuf Process* **2013**, 28, 761.
- [104] G. Ali, F. Butera, N. Rotundo, *J Comput Electron* **2014**, 13, 323.
- [105] R. Rahmani, H. Karimi, L. Ranjbari, M. Emadi, M. Seyedmahmoudian, A. Shafabady, R. Ismail, *Plasmonics* **2015**, 10, 495.
- [106] B. Lakehal, Z. Dibi, N. Lakhdar, Presented in part at the 2017 International Conference on Green Energy & Conversion Systems (Gecs), **2017**.
- [107] S. Cicic, S. Tomic, *Sol Energ Mat Sol C* **2018**, 181, 30.
- [108] N. Prodanovic, J. Radovanovic, V. Milanovic, S. Tomic, *J Appl Phys* **2011**, 110, 063713.
- [109] F. Djeflal, T. Bendib, D. Arar, Z. Dibi, *Mater Sci Eng B-Adv* **2013**, 178, 574.
- [110] K. Jager, L. Korte, B. Rech, S. Albrecht, *Opt Express* **2017**, 25, A473.
- [111] K. Bittkau, T. Kirchartz, U. Rau, *Opt Express* **2018**, 26, A750.
- [112] S. S. Han, L. Cai, G. S. May, A. Rohatgi, *leee T Semiconduct M* **1996**, 9, 303.
- [113] L. Cai, S. Han, G. May, S. Kamra, T. Krygowski, A. Rohatgi, *J Electron Mater* **1996**, 25, 1784.
- [114] L. Cai, A. Rohatgi, S. Han, G. May, M. Zou, *J Appl Phys* **1998**, 83, 5885.
- [115] L. C. K. Liao, C. J. Huang, C. C. Chen, C. S. Huang, C. T. Chen, S. C. Lin, L. C. Kuo, *Sol Energ Mat Sol C* **2002**, 71, 169.
- [116] B. Kim, S. S. Han, T. S. Kim, B. S. Kim, I. J. Shim, *leee T Plasma Sci* **2003**, 31, 317.
- [117] B. Kim, D. W. Kim, S. S. Han, *Vacuum* **2004**, 72, 385.
- [118] B. Kim, S. Kim, W. S. Hong, *Plasma Chem Plasma P* **2004**, 24, 29.
- [119] D. Kim, B. Kim, D. Han, N. G. Yoon, *Mater Manuf Process* **2011**, 26, 1248.
- [120] S. J. Lee, B. Kim, S. W. Baik, *Expert Syst Appl* **2011**, 38, 11437.
- [121] S. Lee, A. Pandey, D. Kim, A. Rohatgi, G. S. May, S. Hong, S. Han. Adv Neural Net - Isnn 2007, Pt 3, Proc **2007**, 4493, 246.
- [122] H. S. Kim, B. G. Morris, S. S. Han, G. S. May, Presented in part at the 2008 leee International Joint Conference on Neural Networks, Vol 1–8, **2008**.
- [123] H. S. Kim, S. J. Hong, S. S. Han, Presented in part at the 2009 leee International Conference on Fuzzy Systems, Vol 1–3, **2009**.
- [124] M. Muszyfaga-Staszuk, R. Honysz, *Arch Metall Mater* **2015**, 60, 1673.
- [125] H. Bae, T. R. Jeon, S. Kim, H. S. Kim, D. Kim, S. S. Han, G. S. May, *Soft Comput* **2010**, 14, 161.
- [126] H. Bae, T. R. Jeon, S. Kim, S. S. Han, *Int J Control Autom* **2010**, 8, 841.
- [127] S. S. Han, I. Kim, C. You, J. Joung, *Adv Intel Soft Compu* **2012**, 133, 651.
- [128] J. X. Ye, F. Y. Zhang, *Adv Res Indus Information Sys Mat Eng Pts 1–7* **2011**, 204–210, 189.
- [129] T. H. Hou, K. Y. Lin, C. Lin, Presented in part at the 2013 Ninth International Conference on Natural Computation (Icnc), **2013**.
- [130] D. P. Fenning, J. Hofstetter, A. E. Morishige, D. M. Powell, A. Zuschlag, G. Hahn, T. Buonassisi, *Adv Energy Mater* **2014**, 4, 1400459.
- [131] S. Kim, K. S. Sohn, M. Pyo, *Acs Comb Sci* **2011**, 13, 101.
- [132] E. G. Bae, H. Kim, Y. H. Hwang, K. S. Sohn, M. Pyo, *J Mater Chem* **2012**, 22, 551.
- [133] A. Bahramian, *Surf Interface Anal* **2013**, 45, 1727.
- [134] C. F. J. Kuo, H. Q. Vu, D. Gunawan, W. L. Lan, *Opt Laser Technol* **1959**, 2012, 44.
- [135] J. Ulaczyk, K. Morawiec, P. Zabierowski, T. Drobiaz, N. Barreau, *Mol Inform* **2017**, 36, 1600161.
- [136] A. Ariyarat, I. Takenaka, R. Yoshikawa, F. Gillot, S. Shiratori, *Rsc Adv* **2016**, 6, 98052.
- [137] M. Hosseinnazhad, M. R. Saeb, S. Garshasbi, Y. Mohammadi, *Sol Energy* **2017**, 149, 314.
- [138] E. Kayabasi, S. Ozturk, E. Celik, H. Kurt, *Sol Energy* **2017**, 149, 285.
- [139] S. Ozturk, E. Kayabasi, E. Celik, H. Kurt, *J Mater Sci-Mater El* **2018**, 29, 260.
- [140] S. Ozturk, L. Aydin, N. Kucukdogan, E. Celik, *Sol Energy* **2018**, 164, 1.
- [141] S. A. Anwar, M. Z. Abdullah, *Eurasip J Image Vide* **2014**, 15.
- [142] Z. Mahdavi, M. Z. Abdullah, *Iete Tech Rev* **2015**, 32, 428.
- [143] M. Duchamp, M. Lachmann, C. B. Boothroyd, A. Kovacs, F. J. Haug, C. Ballif, R. E. Dunin-Borkowski, *Appl Phys Lett* **2013**, 102, 133902.
- [144] N. Goffin, F. Lisso, A. Simeone, G. Claudio, J. Tyrer, E. Woolley, *Proc Cirp* **2015**, 37, 101.
- [145] Q. Y. Liang, J. Chen, X. Li, Z. Q. Gao, B. X. Mi, Z. H. Yang, *Sci China Phys Mech* **2015**, 58, 1.
- [146] Z. H. Ruan, Y. Yuan, X. X. Zhang, Y. Shuai, H. P. Tan, *Sol Energy* **2016**, 127, 147.
- [147] D. Diego-Vallejo, D. Ashkenasi, A. Lemke, H. J. Eichler, *Spectrochim Acta B* **2013**, 87, 92.
- [148] D. Diego-Vallejo, H. J. Eichler, D. Ashkenasi, Presented in part at the 2012 International Symposium on Optomechatronic Technologies (Isot), **2012**.
- [149] C. S. Lin, C. W. Lin, S. W. Yang, S. K. Lin, C. C. Chiu, *Intell Autom Soft Co* **2013**, 19, 391.